Eur. Phys. J. B **4**, 431–440 (1998)

THE EUROPEAN PHYSICAL JOURNAL B

Phase transition in the Blume-Capel model with second neighbour interaction

M. Badehdah[1], S. Bekhechi[1], A. Benyoussef[1,a], and M. Touzani[1,2]

[1] Laboratoire de Magnétisme et de Physique des Hautes Énergies, Département de Physique, BP 1014, Faculté des Sciences, Rabat, Morocco
[2] Laboratoire des Matériaux, des Sciences et Techniques des Énergies Renouvelables, BP 6207, ENSET, Rabat, Morocco

Received: 3 November 1997 / Revised: 31 March 1998 / Accepted: 7 April 1998

Abstract. A two dimensional antiferromagnetic spin-1 Ising model with negative next- nearest neighbour interaction ($J_2 < 0$) and under an external magnetic field is investigated by two methods: The mean-field theory and Finite-Size-Scaling based on transfer matrix (TMFSS) calculations. The ground state diagrams exhibit several new phases including frustrated ones. At finite temperature we obtain by these two methods quite rich phase diagrams, with several multicritical points. While Mean field approximation yields phase diagrams which are sometimes even qualitatively incorrect, accurate results are obtained from transfer matrix finite size scaling calculations. For a certain range of interaction parameters, the model is shown to violate the ordinary universality hypothesis.

PACS. 75.10 Hk Classical spin models

1 Introduction

The Spin-1 Ising Blume-Capel model [1] and its generalization the Blume-Emery-Griffiths model (BEG) [2] are useful for representing a variety of physical and chemical systems. These models have been proposed to describe superfluidity and phase separation in He^3–He^4 mixtures [2] and ordering in a binary alloy [3]. Various extensions of these models have found applications in the description of the properties of many substances [4].

The Blume-Capel (BC) model has been studied by different methods: mean- field approximation (MFA) [1], effective field theory with differential operator technic [5], Monte-Carlo simulation (MC) [6], transfer-matrix finite-size-scaling (TMFSS) [7], series expansion methods [8] and constant-coupling approximation [9]. All these methods affirm the existence of the tricritical point in the phase diagram.

In the case of a two-dimensional triangular lattice, Collins *et al.* [10] have shown that the $S = 1$ Ising model is equivalent to the three state lattice-gas model used to describe [11] multicomponent chemi- and physisorption problems. They have used TMFSS to obtain adsorption isotherm data which are in good correlation with experimental systems. To model poisoning phenomena, Collins *et al.* [12] has added to this model nearest-neighbour lateral interactions. MC simulation and TMFSS calculations have been used to understand the topological details of the phase transition surfaces that allow the determination of these poisoning criteria. They have shown that these longer interactions strongly affect the global topology of the phase transition surfaces, but they don't destroy the features which cause poisoning effects. New features have been found in the usual BEG model with negative biquadratic interaction. It shows six new topologies with new phases (ferrimagnetic and antiquadrupolar) and multicritical points of higher order [13,14]. Recently Buzano *et al.* [15] added to the usual BEG model a repulsive plaquette interaction and studied it by the cluster variational method on a square lattice, they found new phases in the phase diagrams: a ferrimagnetic and a weakly ferromagnetic phase and several multicritical points. Also, the Blume-Capel model with ferromagnetic second neighbour interaction [16] has been used to explain the dependence of the position of the tricritical point on the relative strength of the second to the first neighbour interactions, in order to describe such behaviour observed in some rare-earth multilayers [17].

The Spin-1 Blume Capel model with ferromagnetic or antiferromagnetic interaction under an external magnetic field [18,19] belongs to the Ising universality with the known critical and tricritical values of critical exponent [20]. The extension of this model to higher spin-order ($S = 3/2$) has led to ferrimagnetic and antiferrimagnetic phases in the phase diagrams with a variety of multicritical points of higher-order within MFA [21]. Numerical studies, by means of TMFSS calculations and MC simulations [22], confirm the main qualitative features of the phase diagrams but with only tricritical and critical end

[a] e-mail: benyous@fsr.ac.ma

points. The critical and tricritical exponent calculations yield that these models also belong to the Ising universality.

It is believed that a non universal behaviour appears when interactions of longer range are added to these models. Indeed, several Ising spin models exhibit under certain conditions non universality, unlikely any explanation is available for such problem. Binder *et al.* [23] have studied the antiferromagnetic spin-1/2 model, with repulsive second-neighbour and a magnetic field interaction by MFA and MC simulation, and have found that the model belongs to the weak Suzuki universality. When the second neighbour interaction is not the same, we have the two dimensional asymmetric next-nearest-neighbour Ising model (ASYNNNI) which has been introduced earlier [24] to explain oxygen ordering in $YBa_2Cu_3O_z$. Bartelt *et al.* [25] have shown that critical properties of this model can be understood by making an analogy with the Ashkin-Teller model. Their TMFSS calculations confirm this picture. They have found that this model exhibits the Ising universality for the tetra-ortho-1/2 and ortho1/2-ortho-1/4 transitions but for the tetra-ortho-1/4 transition it belongs to the universality class of the XY model with cubic anisotropy. Also Aukrust *et al.* [26] have used large scale MC simulation and TMFSSS calculations to confirm these results. As the interaction parameters are varied, new frustrated phases appear in the model. They have been found by Hilton *et al.* [27] who performed exact ground state calculations. They have obtained seven topologically distinct ground state diagrams and by TMFSS methods they have determined the best values of the interaction parameters which fit the experimental data. By using the coherent-anomaly method (CAM), Minami *et al.* [28,29] studied the non universal critical behaviour of the Ising spin-1/2 model with second and four spin interactions.

Our aim in this paper is to study the effect of a repulsive second neighbour interaction on the antiferromagnetic Blume-Capel model under a magnetic field on a two dimensional lattice. As a matter of fact a negative second neighbour interaction introduces frustration which results in new frustrated ground states. For finite temperature some interesting behaviours appear where transitions of second-order and first-order with several multicritical points of higher-order are present in the phase diagrams. Also this model exhibits a nonuniversal behaviour for certain values of the interaction parameters. Two methods are used in this paper, the mean field theory and the Transfer-matrix finite-size-scaling (TMFSS).

The remainder of the paper is as follow: Section 2 is devoted to the model and ground state diagrams. In Section 3 we briefly outline the mean field approximation. the Finite-Size-Scaling theory based on the Transfer-Matrix Calculations is described in Section 4. Results and discussion are given in Section 5. Finally, in Section 6 we give a conclusion.

2 The model and ground state diagrams

The model is defined by the Hamiltonian:

$$H = -J_1 \sum_{\langle i,j \rangle} S_i S_j - J_2 \sum_{\langle i,j \rangle'} S_i S_j + D \sum_i S_i^2 - H \sum_i S_i. \tag{1}$$

Here the spin variables are localized on sites of a square lattice and take the values $1, 0, -1$. The first and the second terms describe the antiferromagnetic coupling ($J_1 < 0$ and $J_2 < 0$) between spins on sites i and j, the first sum $\sum_{\langle i,j \rangle}$ is restricted to nearest neighbour pairs of spins while the second $\sum_{\langle i,j \rangle'}$ is restricted to next-nearest neighbour pairs of spins. The third term describes the single ion anisotropy and the last term represents the effect of an external magnetic field.

In order to obtain the ground state phase diagrams,we decompose the lattice into four sublattices: a, b, c and d, we calculate the energy by plaquette E_p.

$$E_p = -\frac{J_1}{4}(S_aS_b+S_bS_c+S_cS_d+S_dS_a) - \frac{J_2}{2}(S_aS_c+S_bS_d) + \frac{D}{4}(S_a^2+S_b^2+S_c^2+S_d^2) - \frac{H}{4}(S_a+S_b+S_c+S_d) \tag{2}$$

where S_a, S_b, S_c and S_d belong to four different sublattices. Ground state phases are given by configurations minimizing E_p. Boundaries between different regions are obtained by pairwise equaling ground state energies, Figures 1a, b, c.

In the asymptotic strong field limit the Hamiltonian (1), reduces to that of the $S = 1/2$ Ising model under a magnetic field with nearest and next-nearest neighbour interactions

$$\hat{H} = -\hat{J}_1 \sum_{\langle i,j \rangle} \sigma_i \sigma_j - \hat{J}_2 \sum_{\langle i,j \rangle'} \sigma_i \sigma_j - \hat{H} \sum_i \sigma_i. \tag{3}$$

- For $H \to +\infty$, the ground state is ferromagnetic with all spins up, then $S_i = -1$ becomes unfavorable. Thus $S_i = S_i^2$, and the model reduces to the effective $S = 1/2$ Ising model with effective interactions defined by:

$$\begin{aligned} \sigma_i &= 2S_i^2 - 1, \\ \hat{J}_1 &= \frac{1}{4}J_1, \\ \hat{J}_2 &= \frac{1}{4}J_2, \\ \hat{H} &= \frac{1}{2}\big(H - D + 2(J_1 + J_2)\big). \end{aligned} \tag{4}$$

- Analogously, as $H \to -\infty$, the ground state is ferromagnetic with all spins down, and the $S_i = +1$ becomes unfavorable. Thus $S_i = -S_i^2$, and the corresponding effective $S = 1/2$ Ising parameters for this asymptotic limit

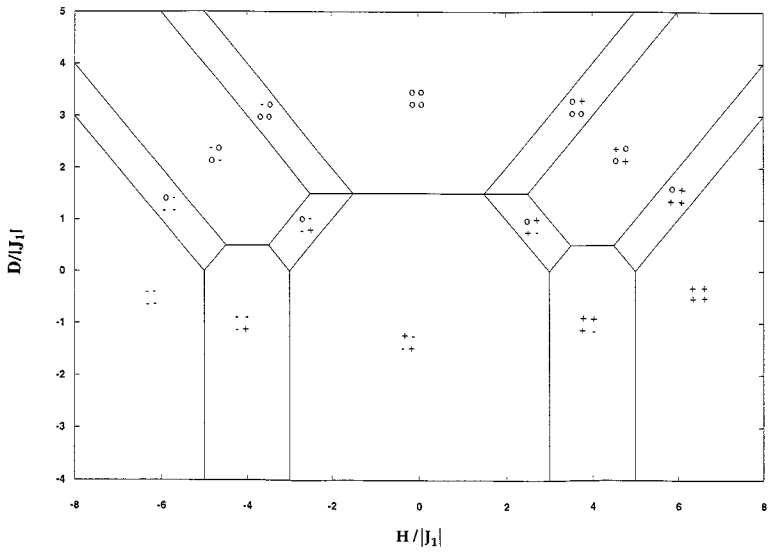

(a)

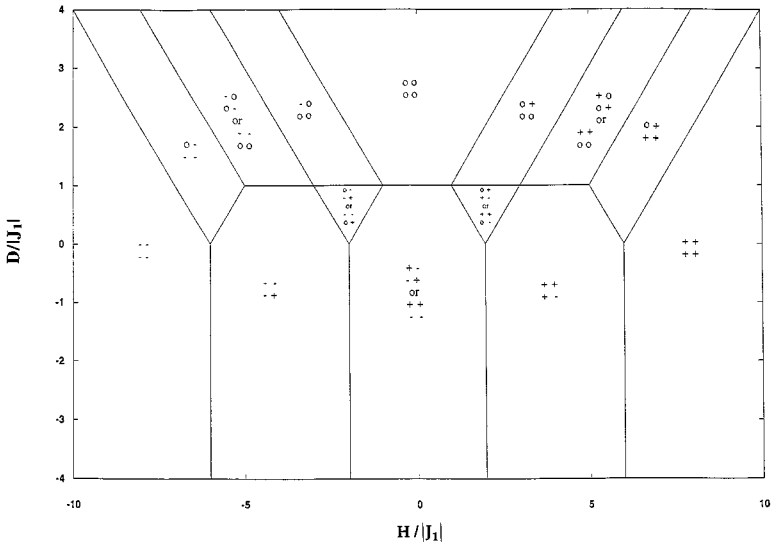

(b)

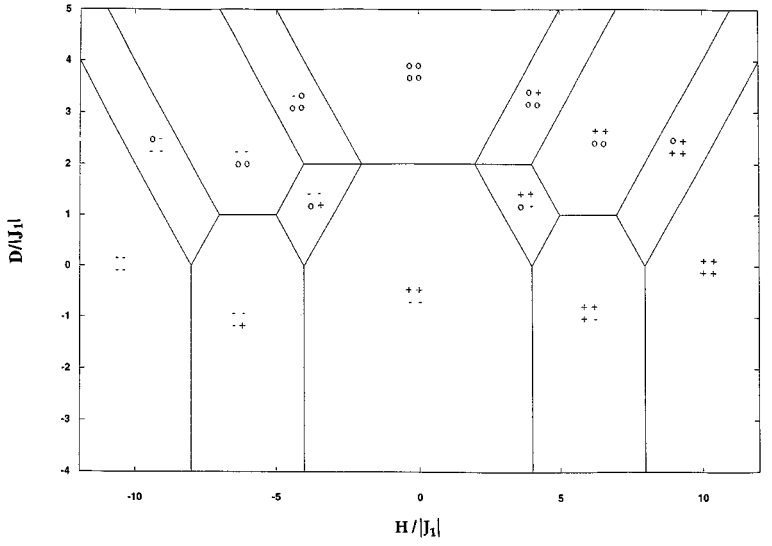

(c)

Fig. 1. Ground State Phase diagrams for: (a) $|J_2| = 1/4$; (b) $|J_2| = 1/2$; (c) $|J_2| = 1$.

are:

$$\begin{aligned}\sigma_i &= 2S_i^2 - 1,\\ \hat{J}_1 &= \frac{1}{4}J_1,\\ \hat{J}_2 &= \frac{1}{4}J_2,\\ \hat{J} &= \frac{1}{2}\big(-H + D + 2(J_1 + J_2)\big).\end{aligned} \tag{5}$$

- For large positive anisotropy ($D \to +\infty$) we have an uniform ground state where all spins are zero, and for large negative ($D \to -\infty$) the state zero becomes unfavorable.
- For $|J_2| = 1/4$ (respectively Strong, $|J_2| = 1$), Figure 1a (respectively Fig. 1c), we have the antiferromagnetic, AF $\begin{smallmatrix}+-\\-+\end{smallmatrix}$, (respectively superantiferromagnetic, SAF $\begin{smallmatrix}--\\++\end{smallmatrix}$) phases, while for intermediate value of J_2, $|J_2| = 1/2$, Figure 1b, the AF and the SAF phases are degenerate.
- For intermediate values of D and H, new phases appear in the phase diagram due to the competition between J_2 and J_1. A highly degenerate structure, $\begin{smallmatrix}++\\+-\end{smallmatrix}$ where ferromagnetic rows alternate with antiferromagnetic ones, with degeneracy 8, is obtained for negative D. While for small positive D and large H we have also another highly degenerate structure, $\begin{smallmatrix}0+\\++\end{smallmatrix}$ with degeneracy 8. These two phases exist in the BEG model with negative plaquette interaction [12]. In addition to these phases, we have also obtained other new degenerate ones. For $|J_2| = 1/4$, Figure 1a, a degenerate phase $\begin{smallmatrix}0+\\+-\end{smallmatrix}$ appears for small positive D and H and by increasing J_2, $|J_2| = 1$, Figure 1c, this phase shifts to $\begin{smallmatrix}++\\0-\end{smallmatrix}$, while for $|J_2| = 1/2$, Figure 1b, these phases are degenerate.

In Figure 1a where J_2 is weak the $\begin{smallmatrix}+0\\0+\end{smallmatrix}$ which exists in the antiferromagnetic Blume Capel model with a magnetic field [18], remains stable for small J_2, but for $|J_2| = 1$ it becomes superantiquadrupolar $\begin{smallmatrix}++\\0\,0\end{smallmatrix}$, where rows of up spins alternate with rows of spins 0, Figure 1c, while for $|J_2| = 1/2$, both phases are degenerate, Figure 1b.

3 Mean-field approximation

We decompose the lattice under consideration into four sublattices $\{\alpha\} = 1, 2, 3, 4$ with corresponding fields $\{H_\alpha\}$ which act on the sites of the αth sublattice only and the ordinary magnetic field is given by:

$$H = \frac{1}{\nu}\sum_{\alpha=1}^{\nu} H_\alpha. \tag{6}$$

Hence the Hamiltonian (1) becomes:

$$H = \sum_{\alpha=1}^{4}\sum_{j\in\alpha} H_\alpha^{eff}\Big(\Big\{s_j\Big\}\Big)s_i = \sum_{\alpha=1}^{4}\sum_{j\in\alpha} J_{ij}s_is_j + H_\alpha \quad i \in \alpha \tag{7}$$

where the average value of H_α^{eff}, is given by:

$$\bar{H}_\alpha^{eff} = H_\alpha + \sum_{\alpha=1}^{4}\sum_{i\in\alpha} J_{ij}\langle s_j\rangle = H_\alpha + \sum_{\alpha=1}^{4}\varepsilon_{\alpha\beta}m_\alpha \tag{8}$$

where m_α and $\varepsilon_{\alpha\beta}$ are respectively the sublattice magnetization and the interaction parameter are given by:

$$m_\beta = \frac{4}{N}\sum_{j\in\beta}\langle s_j\rangle \tag{9}$$

and

$$\varepsilon_{\alpha\beta} = \sum_{j(\neq i)} J_{ij} \quad i \in \alpha,\ j \in \beta. \tag{10}$$

The mean field Hamiltonian then becomes

$$H^{mfa} = \sum_{\alpha=1}^{4}\sum_{i\in\alpha}\Big(\sum_{\beta=1}^{4}\varepsilon_{\alpha\beta}m_\beta + H_\alpha\Big)s_i - \frac{1}{2}\sum_{\alpha=1}^{4}\frac{N}{4}\sum_{\beta=1}^{4}\varepsilon_{\alpha\beta}m_\alpha m_\beta, \tag{11}$$

the free energy is given by:

$$F^{mfa} = -T\ln 2 - \frac{T}{4}\sum_{\alpha=1}^{4}\ln\Big\{2e^{-\frac{D}{T}} \times \cosh\Big(\frac{1}{T}\sum_{\beta=1}^{4}\varepsilon_{\alpha\beta}m_\beta + H_\alpha\Big)\Big\} + \frac{1}{8}\sum_{\alpha=1}^{4}\sum_{\beta=1}^{4}\varepsilon_{\alpha\beta}m_\alpha m_\beta. \tag{12}$$

Sublattice magnetizations are given by:

$$m_\alpha = \frac{\sinh\Big(\frac{1}{T}\sum_{\beta=1}^{4}\varepsilon_{\alpha\beta}m_\beta + H_\alpha\Big)}{\cosh\Big(\frac{1}{T}\sum_{\beta=1}^{4}\varepsilon_{\alpha\beta}m_\beta + H_\alpha\Big) + e^{\frac{D}{T}}} \quad \alpha = 1, ..., 4. \tag{13}$$

The stable solutions of (13) are those which minimize the free energy F^{mfa}. The nature of the transition, as is well known will be determined by the behaviour of the order parameter.

4 Transfer-matrix finite-size-scaling calculations

Detailed description of the phenomenological finite-size-scaling method and transfer-matrix formalism on two-dimensional systems are given in [30,31]. A system of linear size N is used with periodic boundary conditions, here only even values of N are considered to avoid the introduction of interfaces and to preserve the antiferromagnetic phase. With $N' = N+2$ the Nightingale condition [30] for the determination of the critical point K_c becomes:

$$\frac{\xi_N(K_c)}{N} = \frac{\xi_{N+2}(K_c)}{N+2} \tag{14}$$

where $\xi_N(K)$ is the correlation length. The symbol K denotes the set of fields $K = (T, J_2, D, H)$. The nature of the transition (first-order or continuous) is determined by examining the finite-size-scaling behaviour of the persistence length $\tilde{\xi}$ [7,19,22,32]. If the scaled persistence length $\tilde{\xi}/N$ on the transition line is a decreasing function of N then the transition is continuous, otherwise the transition is first-order.

The correlation length and the persistence length are obtained from the three largest eigenvalues of the transfer matrix. In the transfer matrix (TM) method, the lattice is approximated by an $N \times \infty$ lattice with periodic boundary conditions in the finite direction. The full $3^N \times 3^N$ transfer matrix can be block diagonalized using invariance under one step translation in the transverse direction. The symmetric and the antisymmetric blocks, T^S (834×834 for $N = 8$) and T^A (831×831 for $N = 8$), are the only two blocks whose symmetries correspond to ordered phases. We diagonalized them with RS library routines (based on EISPACK routines) on DEC station 5000/200. The diagonalization results in four eigenvalues of interest. The largest eigenvalue of both T^S and the transfer matrix is λ_1^S. By virtue of the Perron-Frobenius theorem, it is positive and nondegenerate. The other three are λ_2^S and λ_3^S, second and third largest eigenvalues of T^S, and λ_1^A, the largest eigenvalue of T^A. λ_3^S and λ_1^A alternate as the second largest eigenvalue of the total transfer matrix. These four eigenvalues give rise to three important lengths. The correlation and the persistence lengths are respectively given by:

$$\xi_1^A = \left(\ln |\lambda_1^S / \lambda_1^A| \right)^{-1} \tag{15}$$

$$\xi_1^S = \left(\ln |\lambda_1^S / \lambda_2^S| \right)^{-1}. \tag{16}$$

And the second persistence length corresponding to T^S is:

$$\xi_2^S = \left(\ln |\lambda_1^S / \lambda_3^S| \right)^{-1}, \tag{17}$$

which remains small and peaks near the transition between ordered phases.

The correlation length exponent ν is obtained following the argument of Nightingale [30] where a field differentiation is used and is given by:

$$\nu = \ln \left(\frac{N \partial \xi_N^{-1}(K_c)/\partial T}{(N+2) \partial \xi_{N+2}^{-1}(K_c)/\partial T} \right) \left(\ln(N/(N+2)) \right)^{-1}. \tag{18}$$

5 Results and discussion

5.1 Phase diagrams

For finite temperature, most of the phase diagrams are economically obtained from the TMFSS calculations with $N/N' = 4/6$ and are compared with those derived from MFA. However, to check the convergence of our results and the finite-size effects, we have used systems with $N/N' = 6/8$ for some values of parameters J_2 and D. In order to describe the different entities in the phase diagrams, we will use Griffiths notations. So following Griffiths [33], we define the critical end-point $B^m A^n$ as the intersection of a number m of lines of second-order and a number n of lines of first-order. The multicritical point B^m is the intersection of a number m of lines of second-order. The n-phase point A^n is the intersection of a number n of lines of first-order. In particular, we denote by C the tricritical point which is the intersection of a line of second-order and a line of first-order. Due to the invariance of the Hamiltonian under the transformation ($H \to -H$, $S \to -S$) we restrict our study to the case $H/|J_1| \geq 0$. Hereafter we list the most interesting diagrams:

1) when the crystal field is absent, $D = 0$, we have:
For $|J_2| = 1/4$, Figure 2a, there is a second-order transition separating the disordered phase from the antiferromagnetic and the degenerate $^{++}_{+-}$ phases. These ordered phases are separated by a second-order transition as determined from the behaviour of the persistence length [22,32]. These lines meet at a multicritical point B^3. At the intermediate value of $|J_2| = 1/2$, Figure 2b, the antiferromagnetic phase disappears and we have only the degenerate phase $^{++}_{+-}$, which is separated from the disorder by a critical line. While for $|J_2| = 1$, Figure 2c, the disorder is separated from the superantiferromagnetic $^{++}_{--}$ and the degenerate $^{++}_{+-}$ phases by a first-order transition line which meets for high magnetic field a second-order transition line at a tricritical point. These two ordered phases are separated by a first-order transition line.

2) We investigate modifications occurring in phase diagrams when the single ion anisotropy is applied.
- For $|J_2| = 1/4$ and $D = 1$, TMFSS calculations, Figure 3a, yields a quantitative phase diagram more accurate than mean field results, Figure 3b. TMFSS yields only a second order transition separating the disorder from ordered phases $^{+-}_{-+}$, $^{+0}_{0+}$ and $^{0+}_{++}$ for low, intermediate and high magnetic field respectively. The inside phase $^{0+}_{+-}$ is surrounded by a first-order transition line, as well as the transition line between the antiferromagnetic $^{+-}_{-+}$ and $^{+0}_{0+}$ phases, this line is limited by a triple point A^3 and a critical end point B^2A^1. Whereas MFA gives a first order line for low and high magnetic field with multicritical points of higher order. Ordered phases $^{+-}_{-+}$ and $^{+0}_{0+}$ are separated by a first-order transition from TMFSS whereas it is of second order from MFA. Also in the TMFSS calculations the disordered phase extends to the temperature and separates the phase $^{+0}_{0+}$ from $^{0+}_{++}$, phase. This feature is correct because at $H = 5$, there are at $T = 0$ an infinite number of states on an infinite lattice that are degenerate in energy. Whereas MFA does not take into account this degeneracy.
- For $|J_2| = 1/2$ and $D = 1/2$, there is a degeneracy between phases appearing for $|J_2| = 1/4$ and $|J_2| = 1$. TMFSS, Figure 4a, yields a second order transition separating the disordered from ordered phases $^{0+}_{+-}$ or $^{++}_{0-}$, $^{++}_{+-}$,

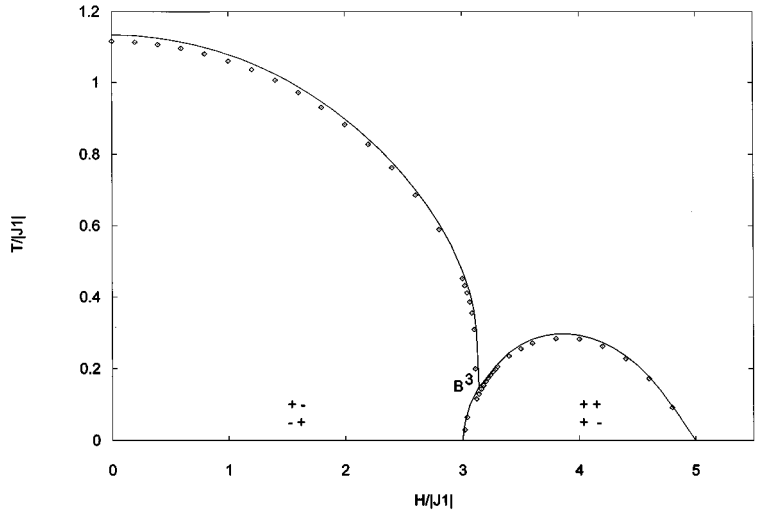

(a)

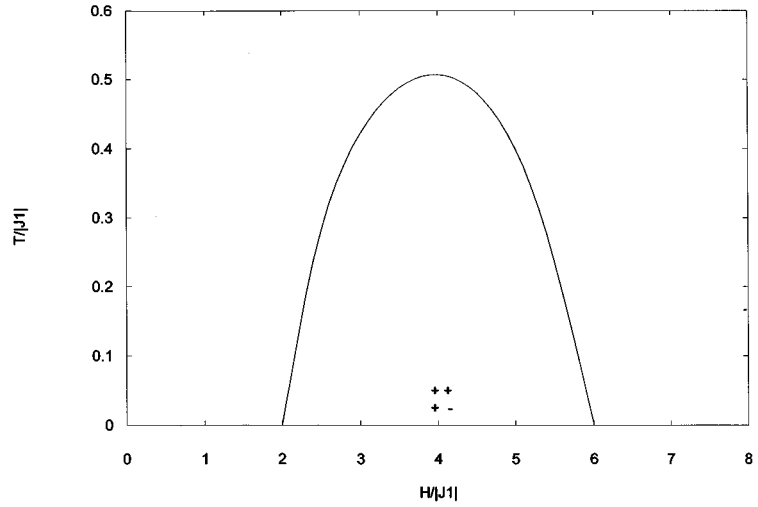

(b)

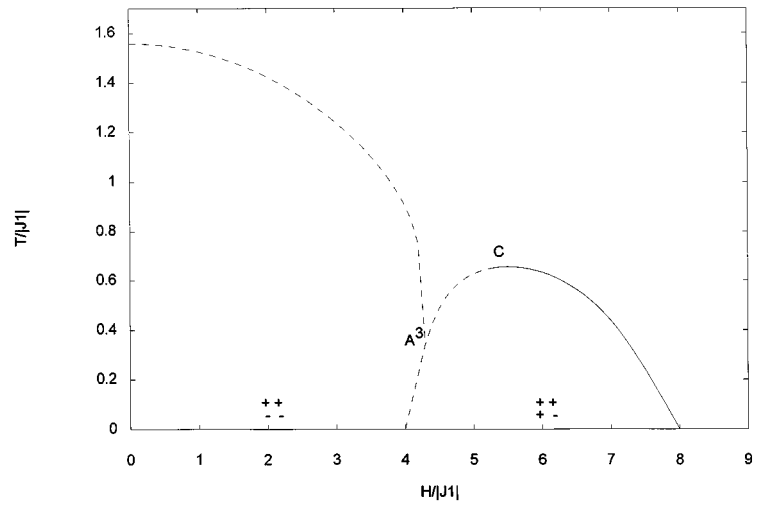

(c)

Fig. 2. Phase diagrams for $D = 0.0$ as obtained from TMFSS with $N/N' = 4/6$. Continuous and dashed lines denote second and first-order transitions respectively. (a) $|J_2| = 1/4$. Calculations with $N/N' = 6/8$ are also added to check convergence. A multicritical point B^3 occurs; (b) $|J_2| = 1/2$; (c) $|J_2| = 1$. A tricritical point C and a triple point A^3 occur.

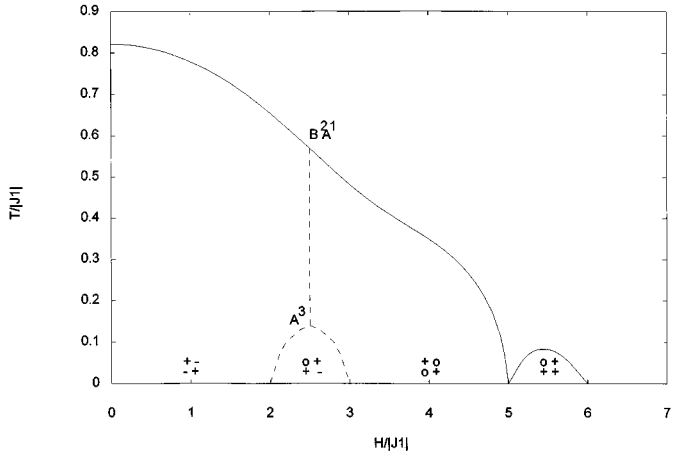

(a)

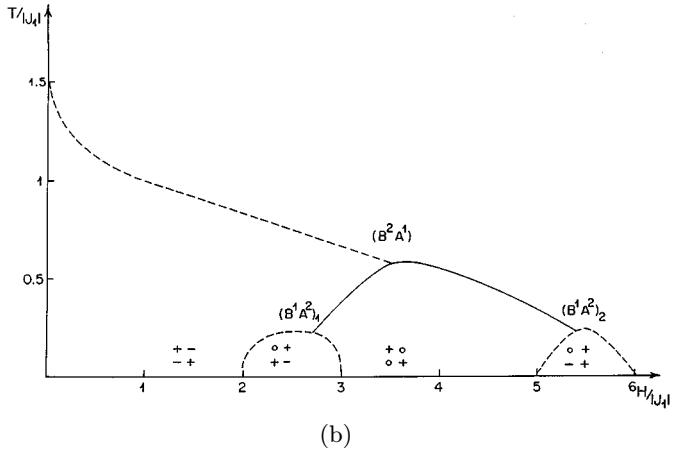

(b)

Fig. 3. Phase diagrams for $|J_2| = 1/4$ and $D = 1.0$ as obtained from: (a) TMFSS with $N/N' = 4/6$. There is a critical end-point B^2A^1 and a triple point A^3. (b) Mean field approximation. Continuous and dashed lines denote second and first-order transitions respectively. There are three critical endpoints B^2A^1, $(B^1A^2)_1$ and $(B^1A^2)_2$.

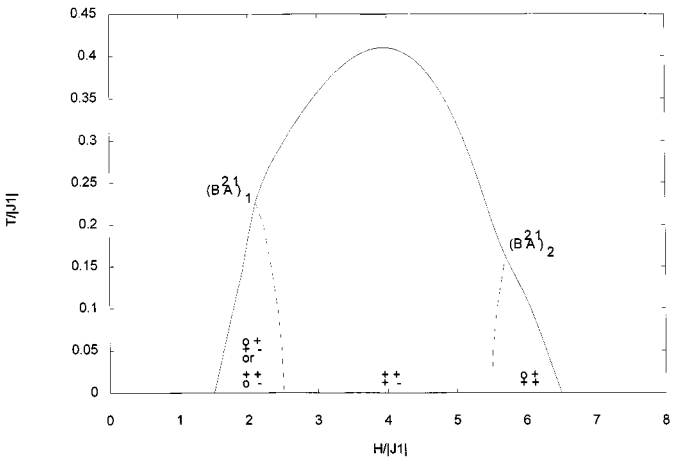

(a)

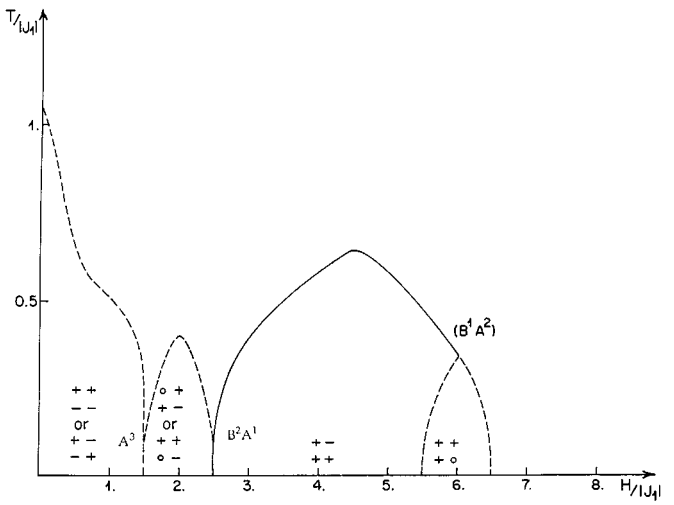

(b)

Fig. 4. Phase diagrams for $|J_2| = 1/2$ and $D = 0.5$ as obtained from: (a) TMFSS with $N/N' = 4/6$. There are two critical end-points $(B^2A^1)_1$ and $(B^2A^1)_2$. (b) Mean field approximation. Continuous and dashed lines denote second and first-order transitions respectively. There are two critical endpoints B^2A^1 and B^1A^2 and a triple point A^3.

$\begin{smallmatrix}0+\\++\end{smallmatrix}$. These phases are separated from each other by a first order transition as determined from the second persistence length. MFA, Figure 4b, results in a phase diagram different from the TMFSS calculations. There is a first order transition separating ($\begin{smallmatrix}++\\--\end{smallmatrix}$ or $\begin{smallmatrix}+-\\-+\end{smallmatrix}$), ($\begin{smallmatrix}0+\\+-\end{smallmatrix}$ or $\begin{smallmatrix}++\\0-\end{smallmatrix}$) and $\begin{smallmatrix}0+\\++\end{smallmatrix}$ phases from the disordered phase for low and high magnetic field respectively. For intermediate values of H, a critical line separates the disordered phase from the degenerate $\begin{smallmatrix}++\\+-\end{smallmatrix}$, phase. There is no finite-temperature transition by TMFSS calculations at low magnetic field from ($\begin{smallmatrix}++\\--\end{smallmatrix}$ or $\begin{smallmatrix}+-\\-+\end{smallmatrix}$) states which exist as ground states of the model. We believe that it's due to the frustration effects (J_2) which disorder the system whereas the magnetic field is too small to order the system. That is why MFA results in a wrong topology for the phase diagram at low H.

- For $|J_2| = 1/4$ and $D = 2$, MFA gives a phase diagram, Figure 5b, where for low H the $\begin{smallmatrix}0+\\0\,0\end{smallmatrix}$ phase confined in the $\begin{smallmatrix}+0\\0+\end{smallmatrix}$ phase. A first-order transition line meets the critical line at a tricritical point and separates the disorder from the $\begin{smallmatrix}+0\\0+\end{smallmatrix}$ phase. For high H, there is a block of critical points separating the $\begin{smallmatrix}0+\\++\end{smallmatrix}$ phase from the $\begin{smallmatrix}+0\\0+\end{smallmatrix}$ phase and the disordered phase. TMFSS results in a phase diagram, Figure 5a, decomposed into three blocks of second-order transition separating ordered phases from the disorder which extends to $T = 0$ between ordered phases. This latter effect is explained by the fact that at $H_1 = 3$ and $H_2 = 6$, there are at $T = 0$ an infinite number of states on an infinite lattice that are degenerate in energy.

- For $|J_2| = 1$ and $D = 3.0$, TMFSS, Figure 6a and MFA, Figure 6b, both yield roughly similar phase diagrams.

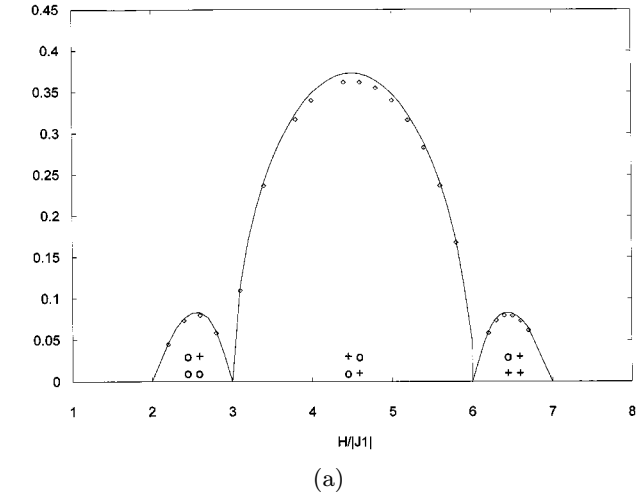

(a)

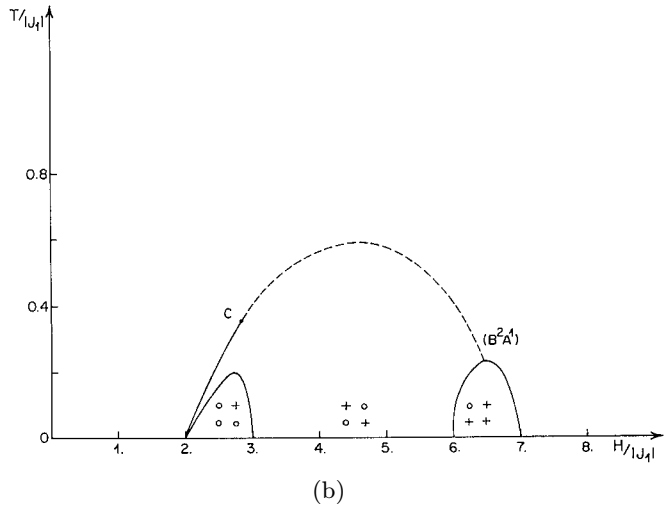

(b)

Fig. 5. Phase diagrams for $|J_2| = 1/4$ and $D = 2.0$ as obtained from: (a) TMFSS with $N/N' = 4/6$ and $N/N' = 6/8$, all transitions are of second-order. (b) Mean field approximation. Continuous and dashed lines denote second and first-order transitions respectively. A tricritical point C and a critical endpoint B^1A^2 occur.

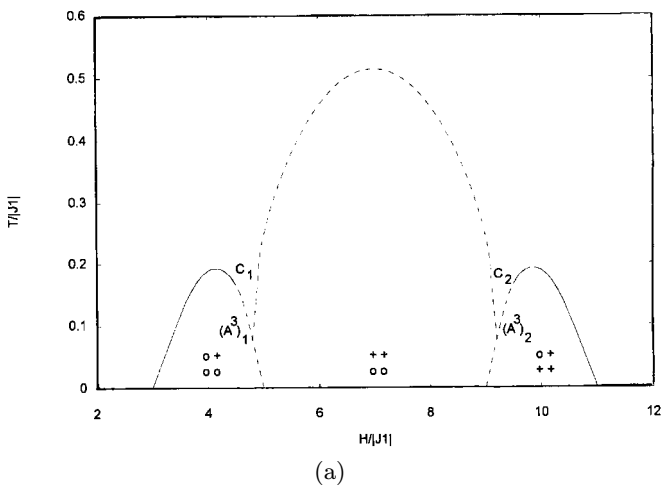

(a)

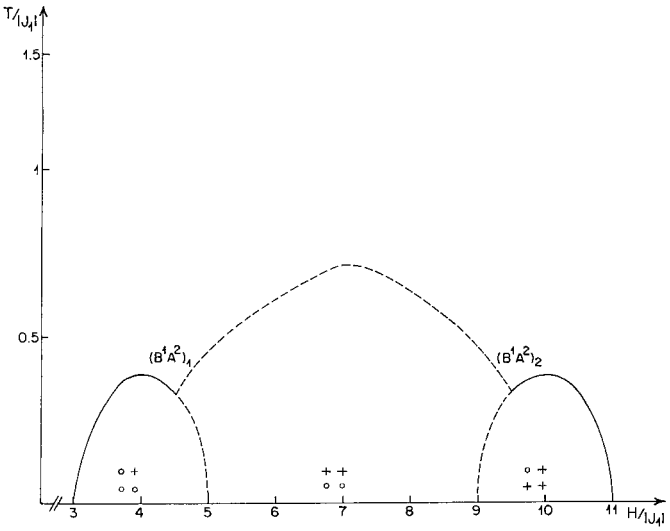

(b)

Fig. 6. Phase diagrams for $|J_2| = 1$ and $D = 3.0$ as obtained from: (a) TMFSS with $N/N' = 4/6$. There are two triple points $(A^3)_1$ and $(A^3)_2$, and two tricritical points C_1 and C_2. (b) Mean field approximation. Continuous and dashed lines denote second and first-order transitions respectively. Two critical endpoints $(B^1A^2)_1$ and $(B^1A^2)_2$ occur.

The $\begin{smallmatrix}++\\0\,0\end{smallmatrix}$ becomes more stable and is separated by a line of first-order from the disordered and the ordered phases. Ordered phases $\begin{smallmatrix}0+\\0\,0\end{smallmatrix}$ and $\begin{smallmatrix}0+\\++\end{smallmatrix}$ are separated from the disordered phase by second order transition from MFA results while TMFSS gives tricritical points. TMFSS gives triple (A^3) and tricritical (C) points while MFA gives only multicritical points of higher order B^1A^2.

5.2 Critical behaviour

In the preceding section we have concentrated on describing the general characteristics of phase diagrams which result from the application of a single ion anisotropy and varying values of $|J_2|$. To discuss the critical behaviour of this model, we have calculated the exponent ν from equation (18) with $N/N' = 4/6$ and $N/N' = 6/8$.

Estimated values of ν at $|J_2| = 1/4$ and $D = 0$, Figure 7a, are consistent with the Ising value of 1 along the critical line separating the antiferromagnetic phase from disorder. At the value ($H_p = 3.18$, $T_p = 0.1540$) where a multicritical point occurs, ν drops to 0.7157 from 6/8 results. For high H and low temperature, ν seems to vary continuously with the magnetic field. This variation is similar for the 4/6 and 6/8 estimates, suggesting that it is not a finite-size-effect and suggesting that ν should be nonuniversal. Such features are similar to those obtained by Aukrust *et al.* [26] for the ASYNNNI Ising model.

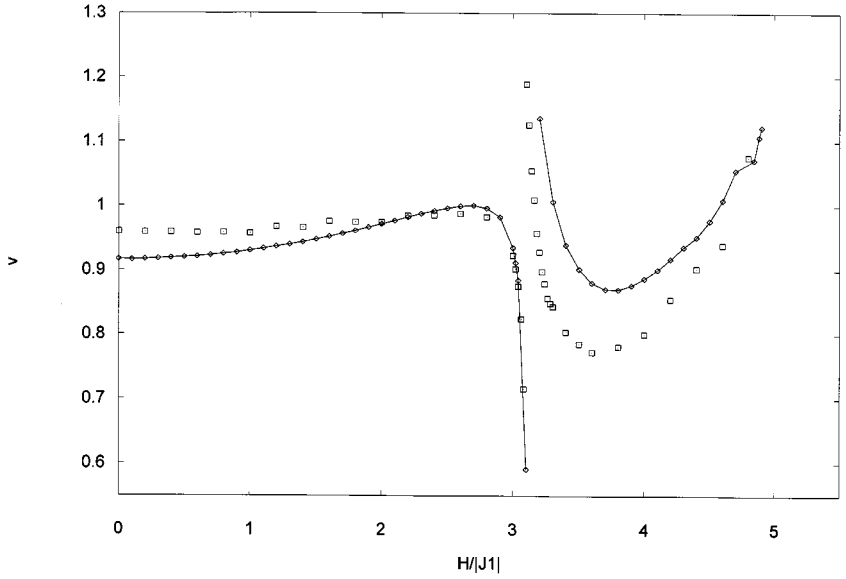

(a)

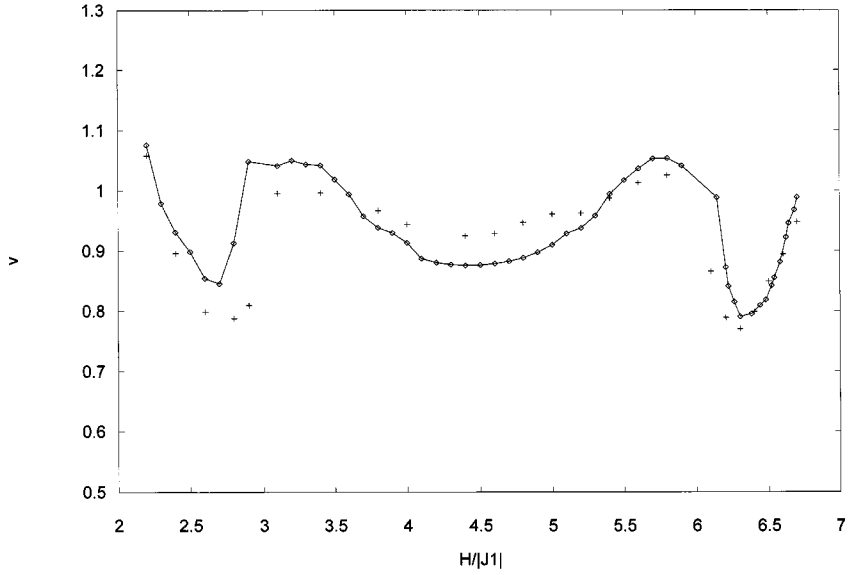

(b)

Fig. 7. Estimates of the critical exponent ν as a function of the magnetic field H, calculated from the TMFSS for different values of the interactions parameters. (a) $|J_2| = 1/4$ and $D = 0.0$, with $N/N' = 4/6$ (diamonds $\diamondsuit$) and $N/N' = 6/8$ (squares). Lines are guides to the eye. (b) $|J_2| = 1/4$ and $D = 2.0$, with $N/N' = 4/6$ (diamonds $\diamondsuit$) and $N/N' = 6/8$ (plus $+$). Lines are guides to the eye.

They concluded that at their multicritical point, their estimate of the exponent ν is close to the value $2/3$ expected for the four state Potts model. Also in our case the $6/8$ result of ν is close to the value $2/3$ but large system sizes are needed to confirm this effect.

For $|J_2| = 1/4$ and $D = 2$, estimates of ν, Figure 7b, suggest also a nonuniversal behaviour of ν along the two critical blocks separating the disordered from the ordered degenerate phases $\begin{smallmatrix} 0 & + \\ 0 & 0 \end{smallmatrix}$ and $\begin{smallmatrix} 0 & + \\ + & + \end{smallmatrix}$, whereas it is Ising like along the block separating the disorder from the $\begin{smallmatrix} + & 0 \\ 0 & + \end{smallmatrix}$ phase.

6 Conclusion

In this paper, we have studied the antiferromagnetic Blume-Capel model with negative next nearest-neighbour interaction and a magnetic field. The ground state phase

diagrams show new phases with frustrated ones due to the competition between the first and second interactions. Our model contains some frustrated phases found by Buzano *et al.* [15] and presents also other new frustrated phases. For finite temperature we have used two methods: mean field approximation (MFA) and finite-size-scaling theory based on transfer matrix (TMFSS) calculations. The MFA gives rich phase diagrams with second-order and first-order transitions. In the phase space (T, D, H), the first and second order surfaces meet at multicritical lines. The limitation of the MFA is that it ignores fluctuations which are very strong in two dimensions but it would be correct for higher dimensions [23]. Also the MFA fails to account for vanishing ordering due to degeneracy effects which make some of the transition temperatures go to zero. It predicts ordered phases for $|J_2| = 1/2$, thus resulting in wrong topologies of the phase diagrams. So we have applied TMFSS calculations in order to take into account the fluctuations neglected by MFA. The phase diagrams are more accurate and qualitatively better than those obtained by MFA. Only in certain regions of J_2, D and H the critical behaviour has been analyzed by calculating the exponent ν, for some values of parameters space. TMFSS with $N/N' = 4/6$ and $6/8$ calculations have shown that the thermal exponent ν varies with the magnetic field for some values of the crystal field D and the second neighbour interaction J_2. Thus suggesting that this model has a nonuniversal behaviour. Finally we hope that this model would provide a rich laboratory for studying a number of phase transitions, critical and multicritical phenomena.

One of the authors, (S.B.) thanks the International Center For Theoretical Physics (I.C.T.P) of Trieste for financial support.

References

1. M. Blume, Phys. Rev. **141**, 517 (1966); H.W. Capel, Physica **32**, 966 (1966).
2. M. Blume, V.J. Emery, R.B. Griffiths, Phys. Rev. A **4**, 1071 (1971).
3. F. Rys, Helv. Phys. Acta. **42**, 606 (1969); A. Hintermann, F. Rys, Phys. Acta. **42**, 608 (1969).
4. G. Grintautas, A. Rosengren, Physica A **208**, 287 (1994).
5. A.F. Siqueira, I.P. Fittipaldi, Physica A **138**, 592 (1986); T.J. Kaneyoshi, Phys. C **19**, L557 (1986); T. Kaneyoshi, Physica A **182**, 436 (1992).
6. B.L. Arora, D.P. Landau, Proc. AIP **5**, 352 (1972).
7. P.D. Beale, Phys. Rev. B **33**, 1717 (1986).
8. J.G. Brankov, J. Przstawa, E. Praveczki, J. Phys. C **5**, 3387 (1972); D.M. Saul, M. Wortis, D. Stauffer, Phys. Rev. B **9**, 4964 (1974).
9. M. Takana, K. Takahachi, Phys. Stat. Sol. B **93**, L85 (1979).
10. J.B. Collins, P.A. Rikvold, E.T. Gawlinski, Phys. Rev. B **38**, 6741 (1988).
11. P.A. Rikvold, J.B. Collins, G.D. Hansen, J.D. Gunton, Surf. Sci. **203**, 500 (1988).
12. J.B. Collins, P. Sacramento, P.A. Rikvold, J.D. Gunton, Surf. Sci. **221**, 277 (1989).
13. W. Hoston, A.N. Berker, Phys. Rev. Lett. **67**, 1027 (1991).
14. S. Lapinskas, A. Rosengren, Phys. Rev. B **49**, 15190 (1994).
15. C. Buzano, L.R. Evangelista, A. Pelizzola, Phys. Rev. B **53**, 15063 (1996).
16. A. Bobak, S. Moscovciak, M. Jurcisin, M. Jascur, Physica A **230**, 703 (1996).
17. C.F. Majkrzak *et al.*, Adv. Phys. **40**, 99 (1991); D.A. Jehan *et al.*, Phys. Rev. B **48**, 5594 (1993).
18. J.D. Kimel, S. Black, P. Carter, Y.L. Wang, Phys. Rev. B **35**, 3347 (1987).
19. J.D. Kimel, P.A. Rikvold, Y.L. Wang, Phys. Rev. B **45**, 7237 (1992).
20. B.M. Mc Coy, T.T. Wu, *The two-dimensional Ising Model* (Harvard University Press, Cambridge, MA, 1973).
21. A. Bakchich, S. Bekhechi, A. Benyoussef, Physica A **210**, 415 (1994).
22. S. Bekhechi, A. Benyoussef, Phys. Rev. B **56**, 13954 (1997).
23. K. Binder, D.P. Landau, Phys. Rev. B **21**, 1941 (1980).
24. L.T. Wille, A. Berera, D. De Fontaine, Phys. Rev. Lett. **60**, 1065 (1988).
25. N.C. Bartelt, T.L. Einstein, L.T. Wille, Phys. Rev. B **40**, 10759 (1989).
26. T. Aukrust, M.A. Novotny, P.A. Rikvold, D.P. Landau, Phys. Rev. B **41**, 8772 (1990).
27. D.K. Hilton, B.M. Gorman, P.A. Rikvold, M.A. Novotny, Phys. Rev. B **46**, 381 (1992).
28. K. Minami, M. Suzuki, Physica A **195**, 457 (1993).
29. K. Minami, M. Suzuki, Physica A **192**, 152 (1993).
30. M.P. Nightingale, Physica A **83**, 561 (1976); Phys. Lett. A **59**, 486 (1977); M.P. Nightingale, J. Appl. Phys. **53**, 7927 (1982).
31. C. Domb, Adv. Phys. **9**, 149 (1960).
32. P.A. Rikvold, W. Kinzel, J.D. Gunton, K. Kaski, Phys. Rev. B **28**, 2686 (1983).
33. R.B. Griffiths, Phys. Rev. B **12**, 345 (1975).